The EMBO Journal (2004) 23, 2488–2497 | © 2004 European Molecular Biology Organization | All Rights Reserved 0261-4189/04
www.embojournal.org

THE EMBO JOURNAL

Two-substrate association with the 20S proteasome at single-molecule level

Silke Hutschenreiter[1], Ali Tinazli[1], Kirstin Model[2] and Robert Tampé[1,*]

[1]Institute of Biochemistry, Biocenter, Johann Wolfgang Goethe-University Frankfurt, Frankfurt a. M., Germany and [2]Department of Structural Biology, Max-Planck-Institute of Biophysics, Frankfurt a. M., Germany

The bipartite structure of the proteasome raises the question of functional significance. A rational design for unraveling mechanistic details of the highly symmetrical degradation machinery from *Thermoplasma acidophilum* pursues orientated immobilization at metal-chelating interfaces via affinity tags fused either around the pore apertures or at the sides. End-on immobilization of the proteasome demonstrates that one pore is sufficient for substrate entry and product release. Remarkably, a 'dead-end' proteasome can process only one substrate at a time. In contrast, the side-on immobilized and free proteasome can bind two substrates, presumably one in each antechamber, with positive cooperativity as analyzed by surface plasmon resonance and single-molecule cross-correlation spectroscopy. Thus, the two-stroke engine offers the advantage of speeding up degradation without enhancing complexity.

The EMBO Journal (2004) **23,** 2488–2497. doi:10.1038/sj.emboj.7600262; Published online 3 June 2004
Subject Categories: structural biology; proteins
Keywords: molecular machines; multicatalytic proteases; protein degradation; self-compartmentalization; single-molecule analysis

Introduction

Different functions can be assigned to self-compartmentalizing machineries in the quality control within the cell (Baumeister *et al*, 1998; Wickner *et al*, 1999; Goldberg, 2003). GroEL/GroES, Hsp60/10 and TRiC are chaperonines facilitating protein refolding, whereas the proteasome, ClpAP, ClpXP and HslVU belong to the proteases degrading abnormal or misfolded proteins. Common to their architecture is the assembly of multisubunit rings to a barrel-shaped complex generating interconnected and functionalized nano-compartments in their interior. The outer rings of most proteases contain ATPase subunits energizing substrate unfolding and translocation into the central chamber, whereas the inner rings catalyze substrate degradation (Wang *et al*, 1997; Hoskins *et al*, 1998, 2000; Singh *et al*, 2000).

*Corresponding author. Institute of Biochemistry, Biocenter, Johann Wolfgang Goethe-University Frankfurt, Marie-Curie Str. 9–11, 60439 Frankfurt a. M., Germany. Tel.: +49 69 798 29476; Fax: +49 69 798 29495; E-mail: tampe@em.uni-frankfurt.de

Received: 24 March 2004; accepted: 10 May 2004; published online: 3 June 2004

The proteasome is nearly ubiquitously distributed among eukarya, archaebacteria and some other prokarya, differing only slightly in subunit sequence (Voges *et al*, 1999). The simplest architecture can be ascribed to the 20S proteasome from archaebacteria like *Thermoplasma acidophilum* (Zwickl *et al*, 1991, 1992; Löwe *et al*, 1995). The evolutionary precursor of all prokaryotic and eukaryotic proteasomes is constructed from only two different subunits, which exhibit high homology due to divergent evolution. Seven α subunits each are assembled in the outer rings, channeling substrates via a central passageway into the degradation chamber, which is encircled by two stacked rings of seven β subunits each. With respect to its $\alpha_7\beta_7\beta_7\alpha_7$ stoichiometry, the barrel-shaped 700 kDa complex is highly symmetrical (D_7 symmetry). Additional regulatory proteins like the proteasome regulator PA700, which mediates unfolding of proteins by hydrolysis of ATP (DeMartino *et al*, 1996; Braun *et al*, 1999; Zwickl and Baumeister, 1999), and the γ-interferon-inducible proteasome activator PA28 associate only with the eukaryotic proteasome (Knowlton *et al*, 1997; Whitby *et al*, 2000). The archaeal homolog to PA700, the proteasome-activating nucleotidase (PAN), has the potential to unfold substrates, but does not necessarily contact the proteasome (Navon and Goldberg, 2001).

The catalytic activity of the proteasome resides in N-terminal threonine residues of the β subunits, which are exposed during autocatalytic processing of their propeptides at the end of assembly (Chen and Hochstrasser, 1996; Ditzel *et al*, 1998). During substrate processing, the threonine residue functions simultaneously as nucleophile and as base due to action of the hydroxyl group and amino group, respectively; thus, the proteasome is a member of the family of N-terminal nucleophile (Ntn) hydrolases (Löwe *et al*, 1995; Seemüller *et al*, 1995). Although the 20S proteasome from *T. acidophilum* differs from any protease of the serine family with respect to the character of the catalytically active centers, it shares the cleavage specificity with chymotrypsin, that is, cuts preferentially behind aromatic amino acids like tryptophane, tyrosine, phenylalanine or the hydrophobic leucine residue (Stein *et al*, 1996; Cardozo *et al*, 1999). In contrast to chymotrypsin, the proteasome displays processivity, as substrates are chopped down to small fragments prior to their release (Akopian *et al*, 1997; Kisselev *et al*, 1998).

Protruding amino termini of the α subunits constrict the narrow entrance channel for substrates into the proteasome interior. Based on mutagenesis, the N terminus of the α3-subunit positions the N termini of the other α subunits, thereby impeding substrate entry into the yeast proteasome, but the constraints can be bypassed by binding of PA700 (Groll *et al*, 2000). In the same manner, docking of PA28-like PA26 induces conformational changes in the α subunits and thus opens the 'gate' (Whitby *et al*, 2000). Due to premature release of the fragments, the product size is increased. Since the eukaryotic 20S proteasome generates antigenic peptides from precursor molecules, the fragment size is optimized for

loading of MHC-class I molecules (Uebel and Tampé, 1999), although trimming by endoplasmic leucine aminopeptidase is often necessary (Harris *et al*, 1992; Beninga *et al*, 1998). Substrates lacking accessible termini can also enter the latent (closed) proteasome after opening of the gate, because they can be cleaved at internal peptide bonds (Liu *et al*, 2003). The entrance channels each dilate into an 'antechamber' juxtaposed to the central cavity. The function of these two antechambers has not been assigned yet. They may play a role in accommodating substrates before their degradation in the central cavity. Furthermore, it is unsettled as to how many substrates associate with the proteasome in one cycle and whether they are degraded simultaneously at the catalytic centers.

One can envisage two basic modes of communication between the central chamber, the antechambers and the internal passageways: Either substrates enter the central cavity of the proteasome through one channel, while products exit through the second channel, or each passageway into the central chamber functions simultaneously as entrance and exit (Köhler *et al*, 2001). Presently, it is not known whether the 20S proteasome works unidirectionally or whether the bipartite structure of the proteasome is somehow correlated with its function. The processive degradation mode might result from its architecture or substrate handling.

To address these questions, we had to disable the functionality of one aperture in order to dissect whether the other pore can compensate for the loss. We chose a novel approach by unique orientation of the proteasome at interfaces, as it is challenging to introduce mutations solely around one pore aperture of the highly symmetrical degradation machinery. We compared for this purpose two recombinant 20S proteasomes, where hexahistidine tags were attached either around the entrances (end-on orientation) or at the sides (side-on orientation). Upon end-on immobilization, processing of one substrate per proteasome could be maintained via the unblocked *cis* aperture. Side-on immobilized and soluble proteasomes can bind two substrates per molecule with positive cooperativity, as demonstrated by surface plasmon resonance and single-molecule analysis.

Results

Activity of His-tagged proteasomes

Recombinant proteasomes were heterologously expressed in *Escherichia coli* and purified via immobilized metal-chelate affinity chromatography and gel filtration. According to SDS–PAGE (Figure 1A) and Western blot (Figure 1B), α N His_6 proteasomes can be clearly separated into two different subunits (His-tagged α subunit: 27 kDa; β subunit: 25 kDa). In the case of β C His_6 proteasomes, the His tag is attached to the smaller subunit. Thus, the two subunits converge in one diffuse band at 26 kDa, which is also detected by the antibodies (antiproteasomal α and β subunit or anti-His tag). In addition to the slight differences in electrophoretic mobility, His-tagged subunits are identified by antiserum against the His tag.

We next tested whether the location of the His tag affects the activity of the proteasome. The release of AMC from the fluorogenic tetrapeptide Suc-LLVY-AMC was measured after terminated incubation with each of the His-tagged proteasomes at 60°C. By linear regression, the fluorescence signal

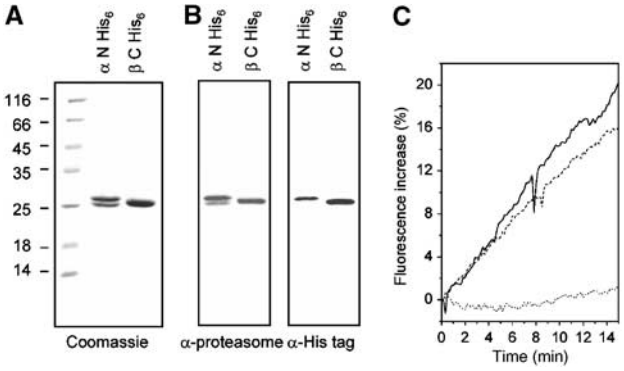

Figure 1 SDS–PAGE, Western blot and proteolytic activity of purified His-tagged proteasomes. (**A**) α N His_6 and β C His_6 proteasomes were separated by SDS–PAGE (15%) and stained with Coomassie brilliant blue. (**B**) α N His_6 and β C His_6 proteasomes were probed by an antibody against the 20S proteasome (lanes 1, 2) and by antiserum against a His tag (lanes 3, 4). (**C**) In homogenous solution, fluorescein-labeled casein (90 nM) was subjected to degradation (15 min, 60°C) by His-tagged proteasomes (7 nM) dissolved in 50 mM Tris, pH 7.5. The fluorescence increase reflecting proteasomal activity is expressed as percentage of the initial fluorescence. The fluorescence increase is denoted as dashed line (β C His_6 proteasome), bold line (α N His_6 proteasome) and dotted line (β T1A proteasome, inactive mutant).

Table I Peptidolytic activities of His-tagged proteasomes

Proteasome	K_M (μM)	K_{cat} (s^{-1})
α N His_6	85.1 ± 5.7	0.054 ± 0.002
α C His_6	38.4 ± 1.5	0.055 ± 0.001
β C His_6	39.9 ± 2.2	0.053 ± 0.002

His-tagged proteasomes (5 μg/ml) were incubated for 30 min at 60°C with different concentrations of Suc-LLVY-AMC (10–350 μM) in HEPES buffer. After stopping the degradation, the release of AMC was determined fluorimetrically. The kinetic parameters were obtained from Eadie–Hofstee plots.

was converted into proteasomal activity. The kinetic parameters k_{cat} and K_M (Table I) were deduced from Eadie–Hofstee plots or obtained from Michaelis–Menten and Lineweaver–Burk plots. The catalytic constants were similar for all three His-tagged proteasomes, indicating that the location of the His tag has only a minor effect on the degradation of peptidic substrates by the proteasome. The affinity for the substrate represented by the Michaelis–Menten constant K_M was slightly reduced in case of the α N His_6 proteasome. Possibly, the confinement of the pores by the His tags slightly restricts substrate entry and thus decreases the effective substrate concentration at the catalytic sites.

Finally, the fluorescence increase reflecting the activity of the proteasome against fluorescein-labeled casein as proteinaceous substrate was compared (Figure 1C). As the proteasome eventually cleaves between the single-fluorescein molecules attached to casein, the self-quenching of the fluorophores is relieved during degradation by the proteasome (Akopian *et al*, 1997). In solution, all His-tagged proteasomes display similar activities against fluorescein-labeled casein. As an internal control, the inactive βT1A proteasome mutant harboring a defect in the catalytic centers showed no increase in fluorescence.

Breaking the D_7 symmetry of the proteasome by orientated immobilization

Electron micrographs reveal two distinct orientations of proteasomes corresponding to the location of their His tags (Figure 2). His tags located at the C termini of the β subunits enforce the proteasomes in side-on orientation at chelating interfaces (Figure 2A). β C His_6 proteasomes appear striated due to the organization in four stacked discs (left). A statistical analysis revealed that less than 2% of all β C His_6 proteasomes are orientated end-on at chelating interfaces (right). Proteasomes with His tags at the N termini of the α subunits are immobilized predominantly end-on at chelating interfaces (Figure 2B and C). Less than 4% of all particles are detected in side-on orientation. Longer adsorption times of the α N His_6 proteasomes to metal-chelating lipid interfaces allow two-dimensional crystallization of the proteasomes (Figure 2C). In the top view, the pore apertures of α N His_6 proteasomes become clearly visible. Wild-type proteasomes without His tags are randomly orientated (Thess *et al*, 2002). Hence, coordination with the chelating interface is mediated specifically via the His tag. Random orientation is also observed, if chelating lipids or nickel ions are missing at the interface.

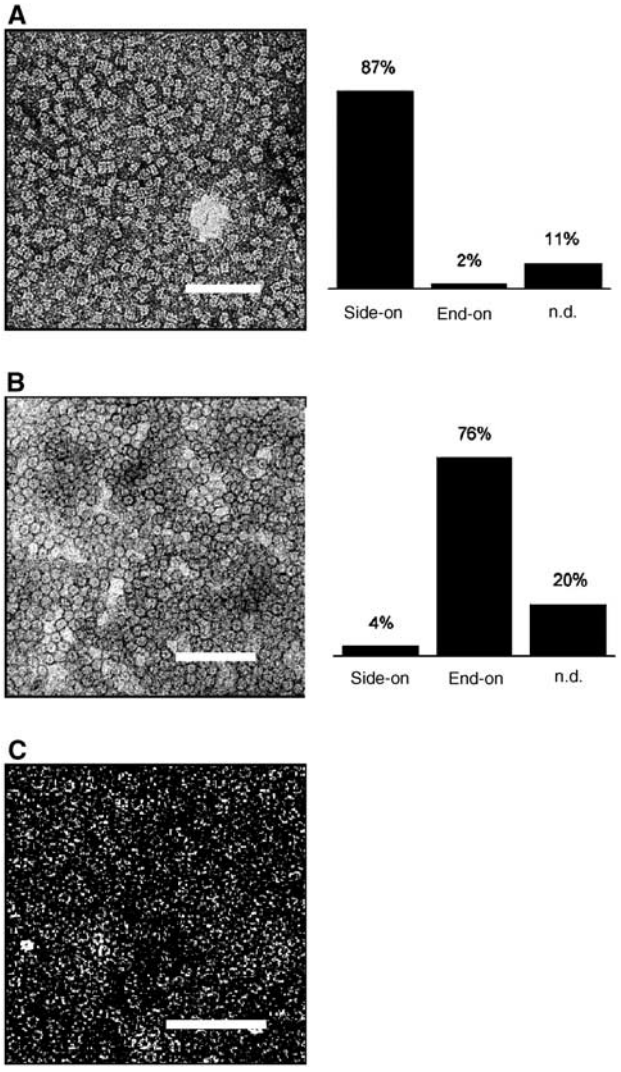

Figure 2 Electron micrographs of two different His-tagged proteasomes displaying two uniform orientations at metal-chelating lipid interfaces. (**A**) β C His_6 proteasomes are enforced in side-on orientations at metal-chelating lipid films. (**B**) α N His_6 proteasomes appear in end-on views at chelating interfaces. Statistics on the orientation of β C and α N His_6 proteasomes are shown in the right panel. (**C**) 2D crystallization of α N His_6 proteasomes in uniform end-on orientation. The scale bars correspond to 50 nm.

Protein degradation by proteasomes is controlled by their orientation

Site-specific orientation of the proteasomes was key to understanding mechanistic aspects. For this purpose, similar amounts of proteasome were immobilized at nickel-chelating lipid interfaces, whereby adsorption was not restricted by crowding, and their activity against fluorescein-labeled casein was studied (Figure 3A). The tight binding of the His tags to the chelator lipids could be reversed by addition of EDTA, and substrate degradation was recorded again with the desorbed proteasomes (Figure 3B). The activity of α N His_6 proteasomes immobilized end-on at the lipid interfaces was enhanced threefold upon desorption of the proteasomes (Figure 3C). The activity of the β C His_6 proteasomes against fluorescein-labeled casein was comparable when immobilized side-on at lipid interfaces and after complete desorption. The fluorescence increase directly reflects the activity of the proteasome (see Figure 1C). Consequently, 'dead-end' proteasomes are able to degrade substrates, albeit at one-third the rate compared to side-on immobilized or soluble proteasomes.

Monitoring substrate loading and unloading of the proteasome in real time

The processing of substrates by the proteasome can be dissected after defined immobilization at metal-chelating interfaces. To follow the interaction of substrates and proteasome in real-time, we applied surface plasmon resonance spectroscopy. α N His_6 and β C His_6 proteasomes were bound site-specifically to NTA thiols integrated in the matrix of the gold chip. The maximum binding values are consistent with a surface coverage of about 20%, assuming molecular areas of 95 nm^2 for the α N His_6 proteasome and of 165 nm^2 for the β C His_6 proteasome. Subsequently, substrate loading and unloading of the 20S proteasome were recorded at increasing concentrations of casein. Substrate association is specific, as casein binding is efficiently competed out by small peptides. The normalized casein resonance signals obtained with α N His_6 and β C His_6 proteasomes (Figure 4A and B, respectively) were plotted against the substrate/proteasome stoichiometry (Figure 4E). Strikingly, the final value of the fit for the substrate/proteasome ratio was about two-fold for the β C His_6 proteasome when compared with the α N His_6 proteasome (1.85 versus 1.14). It can thus be concluded that end-on-immobilized α N His_6 proteasome associates with one substrate, whereas side-on-immobilized β C His_6 proteasome simultaneously binds two substrates. Fitting the substrate/proteasome binding curves with the Hill equation yielded Hill coefficients of 1.4 ± 0.3 and 2.0 ± 0.3 for α N His_6 and β C His_6 proteasomes as rough estimates, respectively. Thus, two-substrate association with β C His_6 proteasomes underlies positive cooperativity in contrast to one-substrate association. The half-saturation constants are similar: 7.7 μM for α N His_6 proteasomes and 7.9 μM for β C His_6 proteasomes. From the dissociation intervals of casein, the k_{off} values can be

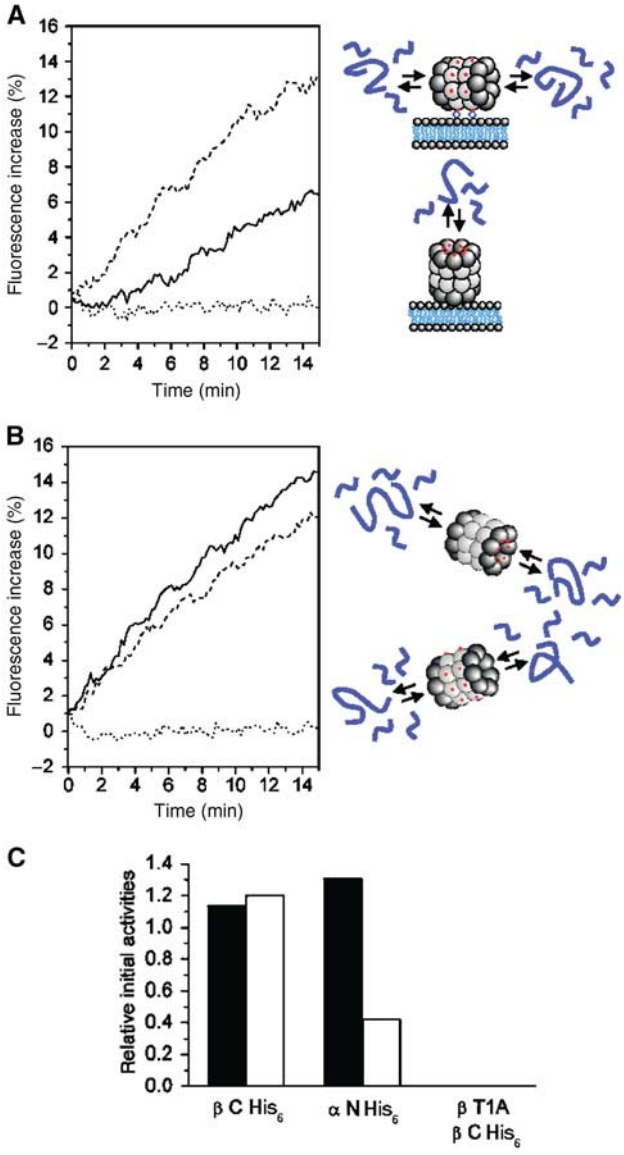

Figure 3 Proteolytic activity of side-on and end-on immobilized proteasomes. His-tagged proteasomes were (**A**) immobilized on or (**B**) desorbed from NTA-lipid vesicles by addition of 100 mM EDTA and dissolved to a final concentration of 7 nM in 50 mM Tris, pH 7.5, containing 90 nM fluorescein-labeled casein. Substrate degradation was recorded fluorimetrically for 15 min at 60°C and expressed as fluorescence increase of the initial value. The fluorescence increase is denoted as dashed line (β C His_6 proteasome), bold line (α N His_6 proteasome) and dotted line (β T1A β C His_6 proteasome). (**C**) The initial degradation rates of corresponding proteasomes are compared before (open bars) and after desorption (filled bars).

determined. β C His_6 proteasomes display a k_{off} of 0.36 s^{-1} for casein, whereas α N His_6 proteasomes can be attributed a k_{off} of 0.18 s^{-1}, that is, half the value. When comparing the two immobilized proteasomes, the number of exit pathways is double in case of β C His_6 proteasomes, indicating that the different off-rates arise from statistics.

Two-substrate association with the proteasome

To confirm that two substrates are simultaneously bound to the 20S proteasome, single-molecule experiments were performed. By means of fluorescence auto- and cross-correlation spectroscopies, we dissected the association process at the proteasome in the first- and second-substrate binding steps and determined equilibrium concentrations of the different species and the corresponding binding constants.

In cross-correlation experiments, auto- and cross-correlation curves of β C His_6 proteasome were monitored in the presence of oregon-green 488-labeled insulin B chain and Alexa 633-labeled insulin B chain (Figure 5). Strikingly, two distinctly labeled substrates were colocalized in the proteasome. Parameters derived from the cross-correlation experiment are compiled in Table II. In addition, equilibrium concentrations of all proteasome-bound species and dissociation constants could be determined according to the reaction scheme given in Figure 6. Oregon-green 488-labeled insulin B chain was predominantly bound to the proteasome (bound fraction: 26.3%, $\tau_D = 42\,\mu s$) over Alexa 633-labeled insulin B chain (bound fraction: 12.9%, $\tau_D = 86\,\mu s$), presumably because the smaller label imposed less steric constraints. Processing of both substrates was accompanied by a pronounced fluorescence increase in the green and red channels. The overall dissociation constant of the two-step process was determined from the concentration of free and bound interaction partners ($K_{D,overall} = 3\,\mu M^2$). Subtraction of double binding events with regard to the cross-correlation product concentration revealed the dissociation constants for the first binding process to the proteasome ($K_{D,Sg} = 4.5\,\mu M$ and $K_{D,Sr} = 11.6\,\mu M$, Table III, Supplementary data). Based on the presumption that the proteasomal affinities of the green substrate relative to the red substrate are identical in the first and second binding steps, the dissociation constants for the homo- and heterobisubstrate binding processes could be calculated ($K_{D,Sg^*Sg} = 510$ nM, $K_{D,Sr^*Sr} = 1.32\,\mu M$, $K_{D,Sg^*Sr} = 660$ nM, $K_{D,Sr^*Sg} = 260$ nM). Remarkably, the affinity for the second substrate is more than a factor of 8 higher than that for the first. Consequently, positive cooperativity of the two-substrate binding processes could be demonstrated. In accordance with previous observations, the concentrations of green mono- and bi-substrate complexes dominated over the red mono- and bi-substrate complexes. The cross-correlation product exhibited a concentration between green-only and red-only bi-substrate:proteasome complexes ($c_{Sg^*Sr^*P} = 168$ pM), and according to the instrumental adjustments a diffusion time ($\tau_D = 369\,\mu s$) between the mono- and bi-substrate:proteasome complexes detected in the green ($\tau_D = 290\,\mu s$) and red channels ($\tau_D = 514\,\mu s$). In summary, the proteasome processes two substrates per degradation cycle with positive cooperative binding characteristics.

Discussion

A major challenge in elucidating the molecular mechanism of substrate processing is to overcome the C_2 symmetry of the eukaryotic proteasome or the D_7 symmetry of the archaebacterial proteasome. In case of success, site-directed introduction of mutations at only one pore aperture could decide about the functional necessity of two entrance channels. Surface engineering leading to unique immobilization appears to be a novel practical approach to elucidate the mechanism of highly symmetric barrel-shaped molecular machines. Occlusion of one pore aperture allows one to gain molecular insights into the handling of substrates and products. For biotinylated GroEL, it could be recently shown that specific interaction with streptavidin at the pore aperture

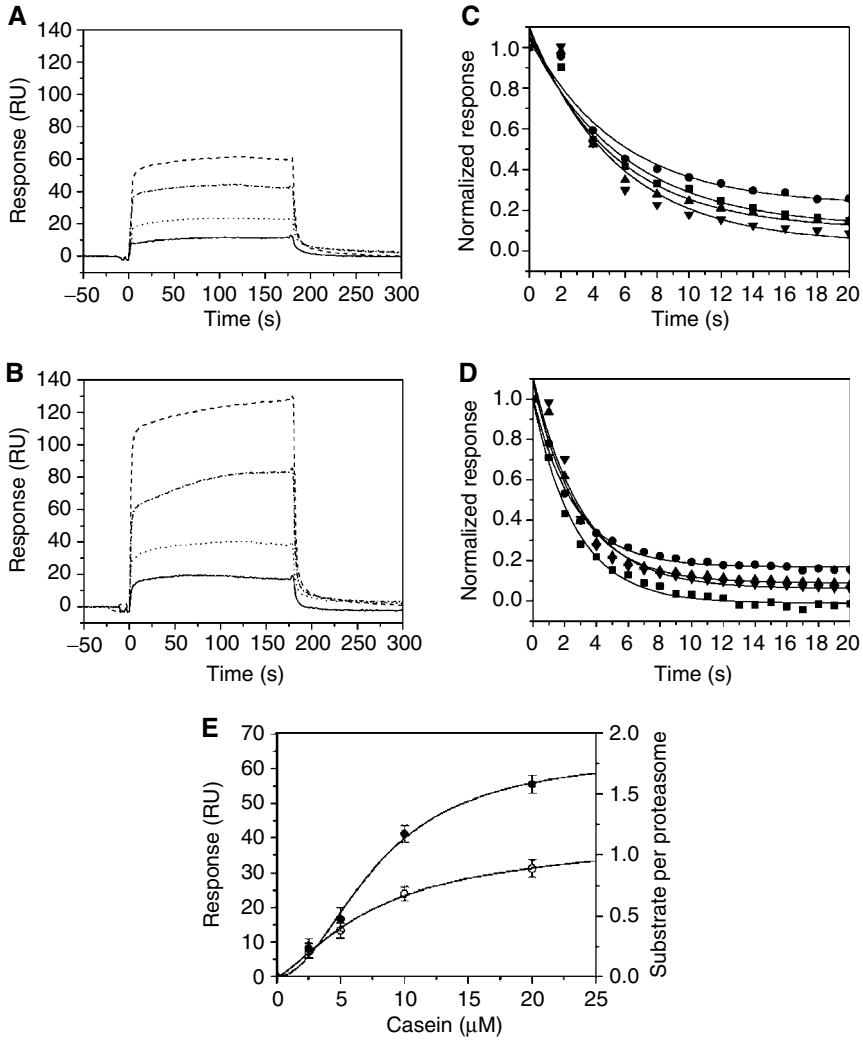

Figure 4 Real-time analysis of substrate association with side-on and end-on immobilized proteasomes. α N His_6 proteasomes (**A**) and β C His_6 proteasomes (**B**) were immobilized in specific orientations at the BIAcore system on a functionalized surface doped with 1 mol% NTA thiols. Subsequently, casein was added as substrate in increasing concentrations of 2.5–20 μM (2.5 μM, bold line; 5 μM, dotted line; 10 μM, dash–dotted line; 20 μM, dashed line). Casein signals were normalized to 1000 RU of immobilized proteasome. Casein dissociation from α N His_6 proteasomes (**C**) and β C His_6 proteasomes (**D**) is depicted after normalization of the signal. The curves are fitted with a monoexponential function within an interval of 20 s. The casein concentrations are denoted as squares (2.5 μM), circles (5 μM), upright triangles (10 μM) and downward triangles (20 μM). (**E**) Stoichiometry of bound casein molecules per immobilized α N His_6 proteasome (open circles) and β C His_6 proteasome (filled circles), respectively. The data were derived from as described in Materials and methods. Data resemble the mean of three measurements.

leads to enclosure of the substrate upon folding; accordingly, the 'Anfinsen cage' model of facilitated substrate refolding was corroborated, while iterative annealing of the substrate could not be accepted for the majority of proteins (Brinker *et al*, 2001).

Here we could demonstrate that the engineered His tags did not interfere with activity of the proteasome. At saturating concentrations of substrate, peptide degradation is not affected by location of the His tag, since catalytic constants are similar for the three differently His-tagged proteasomes. If the concentration of peptidic substrate is rate-limiting, His tags located at the orifices seem to compromise proteasomal activity to a minor extent, as indicated by the elevated Michaelis–Menten constant for the α N His_6 proteasome. In the lower concentration range, restriction of substrate entry into the proteasome might somewhat decrease the effective substrate concentration at the active centers and thus fluorescence increase due to the chymotryptic cleavage site. The degradation of proteinaceous substrates can easily be determined fluorimetrically, since attached fluorophores trigger fluorescence self-quenching relieved upon substrate degradation. The relative activities of different His-tagged proteasomes against peptides and proteins are similar and abrogate any influence of the His tag on the progress of proteolysis.

Scanning force and electron micrographs reveal solely end-on views of α N His_6 proteasomes after immobilization on chelating supports (Thess *et al*, 2002). Thus, the His tags enforce the α N His_6 proteasomes in a uniform orientation, where one pore was occluded by the functionalized interface. We could demonstrate that, with increasing size of the substrate, access of the hidden entrance for the protein becomes more and more restricted. The analysis of substrate binding and product release allows one to distinguish between two alternative models of communication between the

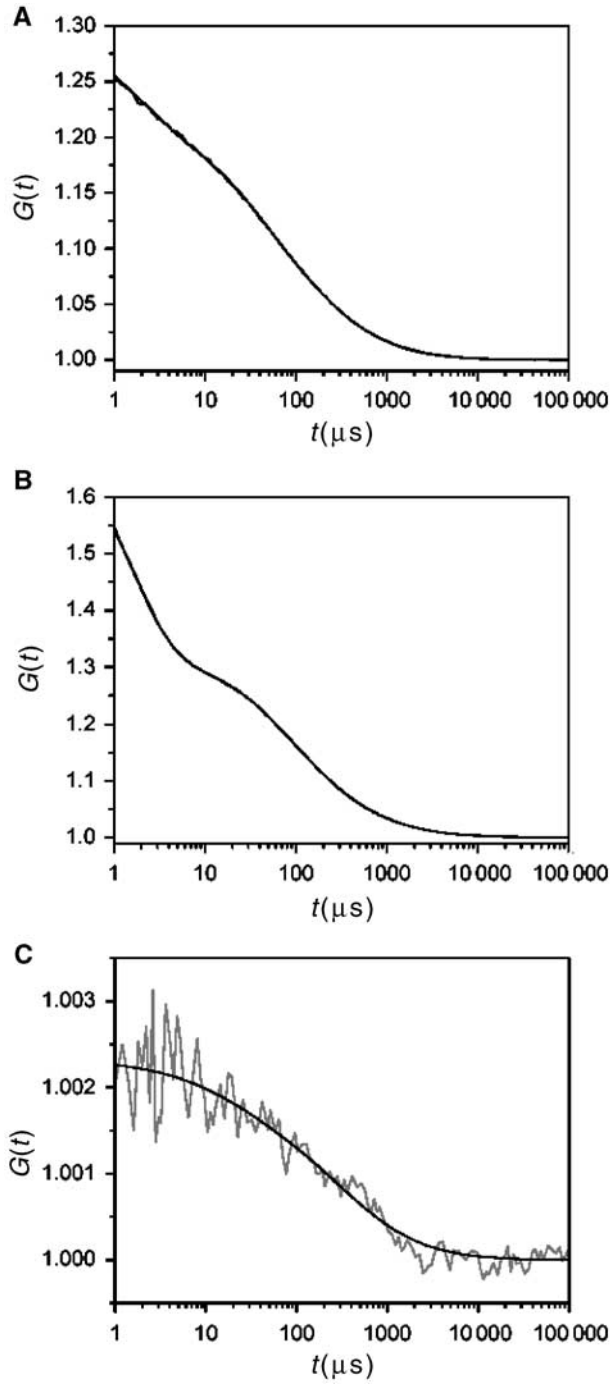

Figure 5 Two-substrate association with the proteasome. Autocorrelation curves ($\lambda_{ex} = 488$ nm (**A**) and $\lambda_{ex} = 633$ nm (**B**)) and cross-correlation curves (**C**) were recorded with β C His_6 proteasome (1.46 μM) and additions of oregon-green 488-labeled insulin B chain (37 nM) and Alexa 633-labeled insulin B chain (22 nM). Auto- and cross-correlation curves were fitted with a two-component model.

Table II Cross-correlation data of two-substrate association with the proteasome

	AC 488	AC 633	CC
τ_{dye} (μs)	21.4	67.2	—
S	5.6	7.9	6.7
V (fl)	0.116	0.540	0.307
$G(0)$	1.224	1.319	1.002
$N_{substrate}$	4.433	2.751	0.031
$c_{substrate}$ (nM)	63.4	8.46	0.168
$\tau_{unbound\ substrate\ or\ dye}$ (μs)	41.5	86.0	22.0
$F_{unbound\ substrate\ or\ dye}$ (%)	73.7	87.1	8.2
$c_{unbound\ substrate\ or\ dye}$ (nM)	46.73	7.37	0.014
$\tau_{bound\ substrate}$ (μs)	290.2±11.8	513.6±27.1	369.2±91.8
$c_{substrate*proteasome}$ (nM)	15.1	0.92	—
$c_{substrate*substrate*proteasome}$ (nM)	1.4	0.005	0.168

Auto- (AC 488 and AC 633) and cross-correlation curves (CC) were recorded with β C His_6 proteasome (1.46 μM) in the presence of oregon-green 488-labeled insulin B chain (37 nM) and Alexa 633-labeled insulin B chain (22 nM). Data were derived from the plots as described in the Materials and methods section or calculated according to the reaction scheme. The cross-correlation curve was background-corrected with regard to a crosstalk of the green emission into the red channel ($Q_{gr} = 8\%$).

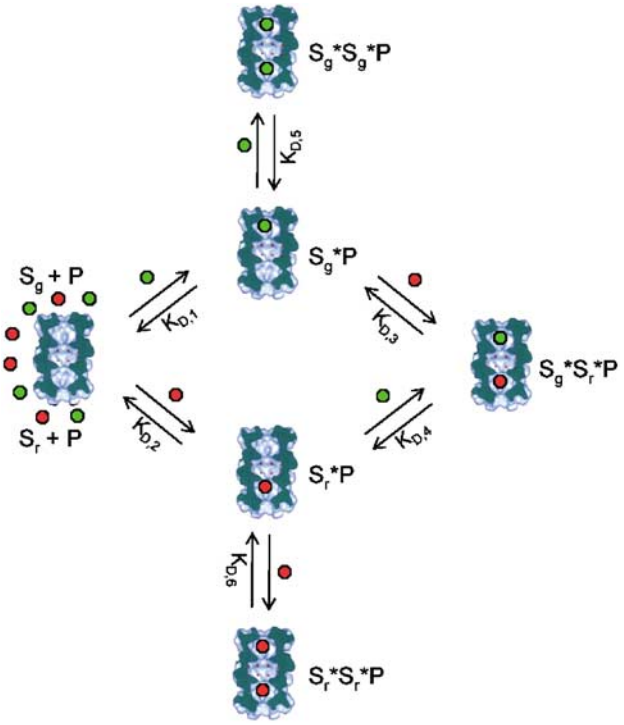

Figure 6 Scheme of the binding events at the proteasome. β C His_6 proteasome (P) binds to oregon-green 488-labeled insulin B chain (S_g) and Alexa 633-labeled insulin B chain (S_r), generating two different single-substrate complexes (S_g*P and S_r*P) and three different binary-substrate complexes (S_g*S_g*P, S_r*S_r*P and S_g*S_r*P). The dissociation constants (K_D) are outlined.

two channels of the proteasome organized in D_7 symmetry. Decreased fragment generation upon immobilization of the α N His_6 proteasome, but not the β C His_6 proteasome, supports influx and efflux of substrates and cleavage products through both apertures of the soluble proteasome. A vectorial model, according to which substrates enter through one pore and products exit through the other one, can also account for the bipartite structure of the proteasome, and proves to be valid if a functional defect is observed upon immobilization.

We studied the activity of proteasomes immobilized uniformly in two orientations. We revealed striking differences dependent on the orientation of the proteasomes. β C His_6 proteasomes immobilized in side-on orientation exceed more than two-fold the activity of immobilized α N His_6 proteasomes.

Table III Dissociation constants of single- and binary-substrate-binding processes

$K_{D,1}$	4.5 μM
$K_{D,2}$	11.6 μM
$K_{D,3}$	660 nM
$K_{D,4}$	260 nM
$K_{D,5}$	510 nM
$K_{D,6}$	1.32 μM

The dissociation constants were calculated according to the reaction scheme (Figure 6).

After complete desorption, the activity of α N His_6 proteasomes is three-fold increased, whereas β C His_6 proteasomes retain their activity. Therefore, the reduced activity of α N His_6 proteasomes is solely due to their unique 'dead-end' orientation. These results document for the first time that one pore is sufficient for substrate entry and product release. In other words, the pore and antechamber can fulfill a triple function in the import and unwinding of substrates and the egress of products.

We next examined the substrate/proteasome stoichiometry by surface plasmon resonance. In case of 'dead-end' orientated proteasome, the maximum ratio of bound casein per immobilized proteasome is approximately one, whereas about two substrates associate with each side-on immobilized proteasome. It is thus reasonable that one substrate enters the central chamber by each of the two pathways. Although theoretically two to three polypeptide chains can concurrently pass the internal channel in case of the end-on immobilized proteasome (Lee *et al*, 2002; Liu *et al*, 2003), our results convincingly demonstrate that this cannot be extended to distinct polypeptides. In addition, the substrate/proteasome-binding behavior indicates significant differences in substrate processing for proteasomes in end-on and side-on orientations. Substrate binding to 'dead-end' orientated proteasomes is associated with a Hill coefficient of ~1, whereas side-on immobilized proteasomes show a Hill coefficient of ~2. Thus, substrate association to proteasomes obeys a two-step process with positive cooperativity. Consequently, 'dead-end' immobilized proteasomes cannot communicate between the *cis* and the blocked *trans* side. Since substrates and degradation products are forced to exit the proteasome in this situation via a single-pore aperture, their dissociation is retarded by a factor of two in comparison to the free proteasome, where two distinct exit pathways are available (two-way traffic). Dissociation from proteasome is apparently not affected by cooperativity. Crevices at the interface between the α and β rings of the *T. acidophilum* proteasome (Groll *et al*, 1997) are too small for the uptake of substrates, but could serve as exits for products. However, the exact 2:1 stoichiometry of the off rates for side-on and end-on immobilized proteasomes indicates that the two terminal pores are the preferential egress pathways.

For multisubunit complexes comprising folding or disassembly machines, a crosstalk between opposite ends has already been observed. Electron microscopy studies with ClpXP revealed alternating translocation of proteinaceous substrates from both ends of the protease and only rare events where both substrates entered the degradation chamber simultaneously through opposite channels (Ortega *et al*, 2002). For the chaperone GroEL, negative cooperativity upon substrate binding in one of the cavities could be directly demonstrated (Falke *et al*, 2001). In case of the 20S proteasome, the observed positive cooperative binding behavior of the second substrate might lead to 'obstruction' of the *trans* side with an entering substrate. Hence, substrates are completely digested in one cycle prior to fragment release, resulting in a unique degradation mode.

Colocalization of substrates in processive machineries can be analyzed on a single-molecule level by fluorescence cross-correlation spectroscopy. Without averaging over an ensemble, single-molecule analyses allow fluctuating systems and subpopulations to be studied under equilibrium conditions. In addition, fluorescence correlation spectroscopy gives valuable information about the binding constants for each subpopulation. Cross-correlation studies demonstrated that two differently labeled insulin B chains are simultaneously bound to the proteasome. In addition to the cross-correlation study, autocorrelation curves were recorded at the individual wavelengths. The autocorrelation data analyzed the binding processes of either oregon-green 488-labeled insulin B chain or Alexa 633-labeled insulin B chain to the proteasome in the steady-state equilibrium. Accordingly, dissociation constants for the two successive binding processes could be derived. The affinity of the second substrate for the proteasome exceeds the affinity of the first substrate by nearly one order of magnitude. Most probably, allosteric interactions account for this phenomenon. Allosteric transitions have already been observed for the proteasome from *Schizosaccharomyces pombe* (Osmulski and Gaczynska, 2000, 2002). In accordance with this model, peptidic substrates may shift the equilibrium from the closed/barrel-like conformation to the open/cylinder-like conformation. Proline- and arginine-rich peptides are known as inhibitors of the allosteric transition (Gaczynska *et al*, 2003). For archaeal proteasomes, a gating mechanism is discussed controversially. For the proteasomal α-ring from *Archaeoglobus fulgidus*, an ordered open conformation could be recently shown in the absence of any activator (Groll *et al*, 2003), which superimposes well with the open conformation of the yeast proteasome. However, the conserved YDR motif of archaeal proteasomes failed to be relevant to a conceivable closed conformation. From mutational studies, it was derived that proteinaceous substrates access the archaebacterial proteasome most efficiently in an open-gate conformation (Förster *et al*, 2003). PAN is assumed to regulate gate opening of the archaeal proteasome (Benaroudj *et al*, 2003). Since the 12 N-terminal residues of each α subunit in the proteasome from *T. acidophilum* are disordered according to the crystal structure (Löwe *et al*, 1995), a gating mechanism for archaeal proteasomes cannot completely be ruled out.

A comprehensive model for the degradation mode of the proteasome has to include the precise temporal and spatial relationship between substrate binding and product release. According to our data, the on-rate for casein binding can be described by a biexponential function, with k_{on} values differing by around one order of magnitude. This conclusion is consistent with the ratio of the dissociation constants for the two binding processes revealed by the cross-correlation studies, if one assumes a fast binding step and a rate-limiting translocation step during association. It is tempting to speculate that the first substrate binds, undergoes translocation, induces pore dilation at both termini during degradation, and consequently facilitates entry of the second substrate into the

proteasome. After processive degradation of the substrates in the central chamber, fragments diffuse passively out of the apertures, thereby re-initiating a new degradation cycle. One can summarize that substrate association with the proteasome underlies an ordered alternating binding mechanism in contrast to the random mode of degradation. The rate-determining step in this cycle is apparently threading of the substrate through the pore followed by translocation, but not proteolytic cleavage. Consequently, a drastic stimulation of activity is expected and observed at elevated temperature for the soluble proteasome compared to the 'dead-end' proteasome. Thus, the two-stroke engine offers the advantage of speeding up degradation without enhancing complexity.

Materials and methods

Materials

Bovine β-casein purified by anion exchange chromatography and bovine insulin were purchased from Sigma. Casein labeled with five to six fluorescein residues per molecule was ordered from Molecular Probes. Oregon-green 488-maleimide and Alexa Fluor 633-C_5-maleimide were from Molecular Probes and Cy5-*N*-hydroxysuccinimidylester (Cy5-NHS ester) was purchased from Amersham Biosciences. The activity of the His-tagged proteasomes was assayed with Suc-Leu-Leu-Val-Tyr-7-amino-4-methylcoumarin (Suc-LLVY-AMC, Bachem, Heidelberg) using 7-amino-4-methylcoumarin (AMC, Sigma) as standard. 1-Stearoyl-2-oleoyl-sn-glycero-3-phosphatidylcholine (SOPC) was a product from Avanti Polar Lipids (Birmingham, AL), while DODA-NTA (N^{α},N^{α}-bis[carboxymethyl]-N^{ε}-[(dioctadecylamino)-succinyl]-L-lysine) was synthesized and characterized as described (Schmitt *et al*, 1994; Dietrich *et al*, 1995).

Expression and purification of proteasomes

Plasmids encoding the proteasomal α and β subunits in tandem under control of the T7 promotor were a kind gift from Drs Erika Seemüller, Andreas Thess and Wolfgang Baumeister (Max-Planck-Institute of Biochemistry, Martinsried). The His tag was attached either to the N or C terminus of the α subunit or the C terminus of the β subunit. In the inactive mutant (β T1A), the catalytically active Thr1 of the β subunit was replaced by Ala (Seemüller *et al*, 1995). The plasmids were transformed into competent *E. coli* BL21(DE3) cells and selected for ampicillin resistance. Positive transformants were grown to midlogarithmic phase ($OD_{600} = 0.6$) for induction of protein expression with 1 mM IPTG (4 h). Harvested cells were lysed by ultrasonication in 50 mM NaP_i, 300 mM NaCl, pH 8.0, after 30 min incubation with lysozyme. The lysate was cleared from cell debris by centrifugation at 37 000 *g*, and applied to a HiTrap Chelating HP column (Amersham Biosciences) preloaded with zinc chloride in the presence of 50 mM NaP_i, 150 mM NaCl, 20 mM imidazole, pH 8.0. His-tagged proteasomes were eluted with 175 mM imidazole in a step gradient. The fractions obtained were concentrated in the presence of 2 mM EDTA in Centriplus (Amicon, Millipore, MWCO: 30 kDa) and loaded on a Superose 6 column (Amersham Pharmacia Biotech) pre-equilibrated with 50 mM NaP_i, 150 mM NaCl, pH 8.0. The proteasome eluted in one peak at 700 kDa.

The purity of the protein was verified by SDS–PAGE (15%). One part of the gel was stained with Coomassie brilliant blue R250, and the other part was blotted on a nitrocellulose membrane. The proteasome was identified with a rabbit antiserum directed against the α and β subunits of the 20S proteasome (gift from Drs Erika Seemüller and Wolfgang Baumeister, MPI of Biochemistry, Martinsried) and a polyclonal HRP-coupled goat-anti-rabbit antiserum (Dianova). The chemiluminescence was developed with the standard system and visualized at the Lumi-Imager (Roche). After stripping, the His-tagged subunits were detected with a mouse antibody against the His tag (Novagen) and a polyclonal HRP-coupled goat-anti-mouse antiserum (Sigma).

Peptidolytic activity of the proteasome

Proteasomes (5 μg/ml) were tested for their activity towards small peptidic substrates by incubating Suc-LLVY-AMC (10–350 μM) for 30 min at 60°C in HEPES buffer (10 mM HEPES, 150 mM NaCl, pH 7.5), quenching the reaction with 100 mM chloroacetic acid, 100 mM acetic acid, pH 4.3, and measuring the release of 7-amino-4-methylcoumarin ($\lambda_{exc/em} = 380/440$ nm). The fluorescence emission was quantified with AMC as standard. The kinetic parameters for α C His_6 and β C His_6 proteasomes referred to substrate concentrations up to 200 μM, because substrate inhibition was observed at higher concentrations.

Electron microscopy of immobilized proteasomes

To demonstrate the specific and uniform orientation of His-tagged proteasomes at metal-chelating interfaces, a Teflon well was filled with 3.5 μg proteasome in 35 μl of HEPES buffer. Subsequently, 1 μl of 1 mM SOPC/DODA-NTA (9:1) in chloroform/hexane (1:1/v:v) was placed on top of the solution. After incubation for 0.5–1 h, the lipid–proteasome assembly was covered with a carbon-coated gold grid for up to 3 min and stained with 1% uranyl acetate. Specimens were investigated in a Philips CM 120 electron microscope (FEI, Eindhoven) operating at 100 kV with a calibrated magnification of × 58 300 under low electron dose conditions covering a defocus range of 1–2 μm. Images were recorded on a Gatan Megascan 2 × 2K CCD camera (Gatan, Inc., Pleasanton, CA) and image quality was assessed by calculating fast Fourier transform (FFT) with Digital Micrograph 3.4.4.

Orientated immobilization of His-tagged proteasomes at metal-chelating lipid interfaces

Lipid films containing 180 μM SOPC, 20 μM DODA-NTA and 20 μM $NiCl_2$ were swollen for 1 h at 37°C in degassed HEPES buffer before repetitive lipid extrusion through polycarbonate membranes (100 nm pore diameter, Avestin, Ottawa, Canada) with a LiposoFast Extruder (Avestin). His-tagged proteasomes were dialyzed overnight against HEPES buffer and incubated for 3 h at 4°C at a final concentration of 160 nM, with the nickel-loaded lipid vesicles in a molar proteasome/chelator lipid ratio of 1:80.

Degradation studies of fluorescein-labeled casein

Fluorescein-labeled casein (90 nM) was adjusted to 60°C in 50 mM Tris, pH 7.5, in a water-jacketed cuvette of the fluorescence spectrometer (Fluorolog III, Horiba). Afterwards, the proteasome immobilized on lipid vesicles was added to a final concentration of 7 nM. As control, His-tagged proteasomes in equivalent concentration were assayed with fluorescein-labeled casein directly in solution or after desorption from lipid interfaces by addition of 100 mM EDTA. Fluorescein-labeled casein bears 5–6 fluorophores per molecule in such an arrangement that cleavage by the proteasome increases the fluorescence by about 20%. The increase in fluorescence reflecting relief of quenching monitors degradation of the substrate and was recorded for 15 min. Initial rate constants were analyzed.

Surface plasmon resonance analysis

Protein binding to a functionalized gold chip was analyzed by surface plasmon resonance at a BIAcore X instrument (BIAcore AB, Uppsala, Sweden). Gold chips were incubated for 24 h in a solution containing 1 mol% NTA-oligoethylene glycol thiol (NTA thiol) and 99 mol% oligoethylene glycol thiol (matrix thiol). The synthesis of the compounds is described separately (manuscript in preparation). The chips were mounted on a plastic holder and ready to use. The BIAcore system was initialized with degassed SPR buffer (10 mM HEPES, 300 mM NaCl, 5 mM imidazole, pH 7.5) at a flow rate of 10 μl/min. With a pulse of 100 mM EDTA, multivalent cations were removed from the surface, followed by uniform loading of the functionalized interface with 100 mM $NiCl_2$. Subsequently, 250 nM of β C His_6 proteasomes or α N His_6 proteasomes was injected over the primed surface until a surface coverage of 1400 resonance units (RU) (β C His_6 proteasome) or 2200 RU (α N His_6 proteasome) was reached, whereby 1000 resonance units RU correspond to a protein concentration of 1 ng/mm^2. To block nonspecific binding, imidazole (20 mM) was added to the proteasome solution. Substrate association and dissociation were recorded at 25°C with injections of up to 20 μM casein, which was previously denatured (60°C, 10 min). The high salt concentration excludes electrostatic binding of the substrate to the charged proteasome surface. To calculate the stoichiometry of substrates per proteasome, the casein signal amplitude was corrected by the refractive index shift and normalized to 1000 RU of immobilized proteasomes, assuming no impact of the orientation parameter. The substrate/proteasome ratio

weighs the normalized signal amplitudes of casein per proteasome with their molecular masses. For k_{off} determination, the casein signal at the end of injection was normalized and fitted with a monoexponential function.

Preparation of fluorescence-labeled insulin B chains

Cross-correlation studies required two photostable, fluorescent substrates, which can be excited at 488 and 633 nm, respectively, without exhibiting a spectral overlap. Thiol-specific labeling was chosen as it guarantees a defined stoichiometry and site specificity. After reduction of insulin with TCEP in degassed citrate buffer (pH 3.0, 30 min, 25°C), insulin B chain was separated by reversed-phase HPLC and identified by MALDI-MS (Voyager De Pro, Perspective Biosystems, Framingham, MA). Reduced insulin B chain with two free cysteines ($M/z = 3400$) was labeled in 50 mM Tris, pH 7.5, with oregon-green 488-maleimide or Alexa Fluor 633-C_5 maleimide, respectively (90 min, 25°C). Labeled insulin B chain was eluted with 38% (v/v) acetonitrile from a μRPC C2/C18 column (Amersham Biosciences). MALDI-MS confirmed two fluorophores per polypeptide chain ($M/z = 4329$ and 5580 for oregon-green 488-labeled insulin B chain and Alexa 633-labeled insulin B chain, respectively). Substrate concentration was determined fluorimetrically.

Cross-correlation experiments

Two laser beams are tightly focused in a spot and excite green- and red-fluorescent molecules upon diffusion into the illuminated volume element. The green ($\lambda_{ex} = 488$ nm) and red ($\lambda_{ex} = 633$ nm) fluorescence signals are dissected and recorded in a time-dependent manner by two highly sensitive photodiodes. Statistical analysis of the individual green- and red-fluorescent events gives rise to two autocorrelation curves, whereas simultaneous events are merged to the cross-correlation curve. The amplitude of the cross-correlation signal indicates the ratio of colocalized green and red species to the ensemble of green and/or red species.

FCS measurements were performed on a Zeiss ConfoCor 2 (Carl Zeiss, Jena) equipped with an argon laser (488 nm, 25 mW) and a helium–neon laser (633 nm, 5 mW). The instrument was controlled by Fluorescence Correlation Microscope ConfoCor 2 software 3.2 FP1 and the auto- and cross-correlation curves were analyzed with Origin 7.0. The pinholes in channels 1 (633 nm, diameter: 90 μm) and 2 (488 nm, diameter: 70 μm) were adjusted with Alexa Fluor 633-C_5 maleimide and fluorescein, respectively. The corresponding confocal volume elements were determined from one-component fits of the respective correlation curves. For cross-correlation experiments, β C His_6 proteasome (1.46 μM) was equilibrated in an eight-well chamber (Nalge Nunc International) to 22°C before adding Oregon-green 488-labeled insulin B chain (20–50 nM) and Alexa 633-labeled insulin B chain (20–50 nM). The red laser was adjusted to a higher intensity than the green laser, thereby minimizing the crosstalk of the green emission into the red channel. Seven independent cross-correlation measurements of 2 min each were averaged. The cross-correlation amplitude exceeded significantly the threshold value of 1.001. The cross-correlation curve was fitted with a two-component model, since the free green fluorophore caused a minor cross-emission into the red channel. The autocorrelation data obtained in the green and red channels were fitted with a two-component model assuming fractions of free and bound substrates. The diffusion times of the free substrates were extracted from one-component fits of an analogous experiment, where oregon-green 488-labeled insulin B chain (20–50 nM) and Alexa 633-labeled insulin B chain (20–50 nM) were monitored in both channels without proteasome. The higher detectable concentration of the free green substrate in comparison with the free red substrate is due to the higher quantum yield of the green dye. Auto- and cross-correlation curves were fitted with a one-component model or a two-component model:

$$G(t) = 1 + \frac{1}{N} \cdot \left(1 + \frac{F \cdot e^{(-t/t_0)}}{1 - F}\right) \cdot \left(\sum_{i=1}^{x} \frac{\Phi_i}{(1 + t/\tau_i) \cdot \sqrt{1 + (1/S^2) \cdot (t/\tau_i)}}\right) \quad (1)$$

with

$$\Phi_i = \frac{Q_i^2 \cdot Y_i}{\left(\sum_{i=1}^{x} Q_i \cdot Y_i\right)^2} \quad \text{and} \quad Y_i = \frac{N_i}{N}$$

x denotes the number of components ($x = 1$ or 2), N the total number of particles in the confocal volume, N_i the number of particles of component i, t the correlation time, τ_i the diffusion time of component i in the confocal volume, F the triplet fraction, t_0 the triplet time, Φ_i the weighting coefficient for the ith component, Q_i the quantum yield of component i, Y_i the relative molecular fraction of component i and S the structural parameter. The axial structural parameter S is introduced for convenience as $S = \omega_2/\omega_1$, where ω_1 is the half short axis (waist radius of the laser beam) and ω_2 the half long axis of the ellipsoidal confocal volume. The particle diffusion time τ through the confocal volume can be described by

$$\tau = \frac{\omega_1^2}{4 \cdot D} \quad (2)$$

where D is the diffusion coefficient of the fluorescent molecule. Diffusion coefficients of $D = 2.80 \times 10^{-10}$ m^2/s for fluorescein and $D = 1.98 \times 10^{-10}$ m^2/s for Alexa Fluor 633-C_5-maleimide were assumed (Carl Zeiss, Jena). In cross-correlation studies, the diffusion time in the confocal volume is the average of the diffusion times in the green and red detection volumes (Supplementary data).

Supplementary data

Supplementary data are available at *The EMBO Journal* Online.

Acknowledgements

We are indebted to Dr K Weisshart, Carl Zeiss, Jena, for guiding the cross-correlation experiments. We thank Åsa Böker and Dr W Kühlbrandt for help with the electron microscopy. We are grateful to Dr R Huber for stimulating discussions. We thank Drs E Seemüller, A Thess and W Baumeister for constructs and antibodies. We acknowledge Drs K Busch, C May and J Reinstein for discussions. We are grateful to Dr U Bahr, Dr M Karas and Jörg Kahnt for discussing the MS measurements. The work was supported by grants from the Volkswagen-Stiftung and the Deutsche Forschungsgemeinschaft.

References

Akopian TN, Kisselev AF, Goldberg AL (1997) Processive degradation of proteins and other catalytic properties of the proteasome from *Thermoplasma acidophilum*. *J Biol Chem* **272:** 1791–1798

Baumeister W, Walz J, Zühl F, Seemüller E (1998) The proteasome-paradigm of a self-compartmentalizing protease. *Cell* **92:** 367–380

Benaroudj N, Zwickl P, Seemüller E, Baumeister W, Goldberg AL (2003) ATP hydrolysis by the proteasome regulatory complex PAN serves multiple functions in protein degradation. *Mol Cell* **11:** 69–78

Beninga J, Rock KL, Goldberg AL (1998) Interferon γ can stimulate post-proteasomal trimming of the N-terminus of an antigenic peptide by inducing leucine aminopeptidase. *J Biol Chem* **273:** 18734–18742

Braun BC, Glickman M, Kraft R, Dahlmann B, Kloetzel PM, Finley D, Schmidt M (1999) The base of the proteasome regulatory particle exhibits chaperone-like activity. *Nat Cell Biol* **1:** 221–226

Brinker A, Pfeifer G, Kerner MJ, Naylor DJ, Hartl FU, Hayer-Hartl M (2001) Dual function of protein confinement in chaperonin-assisted protein folding. *Cell* **107:** 223–233

Cardozo C, Michaud C, Orlowski M (1999) Components of the bovine pituitary multicatalytic proteinase complex (proteasome) cleaving bonds after hydrophobic residues. *Biochemistry* **38:** 9768–9777

Chen P, Hochstrasser M (1996) Autocatalytic subunit processing couples active-site formation in the 20S proteasome to completion of assembly. *Cell* **86:** 961–972

DeMartino GN, Proske RJ, Moomaw CR, Strong AA, Song XL, Hisamatsu H, Tanaka K, Slaughter CA (1996) Identification, purification, and characterization of a PA700-dependent activator of the proteasome. *J Biol Chem* **271:** 3112–3118

Dietrich C, Schmitt L, Tampé R (1995) Molecular organization of histidine-tagged biomolecules at self-assembled lipid interfaces using a novel class of chelator lipids. *Proc Natl Acad Sci USA* **92:** 9014–9018

Ditzel L, Huber R, Mann K, Heinemeyer W, Wolf DH, Groll M (1998) Conformational constraints for protein self-cleavage in the proteasome. *J Mol Biol* **279:** 1187–1191

Falke S, Fisher MT, Gogol EP (2001) Structural changes in GroEL effected by binding a denatured protein substrate. *J Mol Biol* **308:** 569–577

Förster A, Whitby FG, Hill CP (2003) The pore of activated 20S proteasomes has an ordered 7-fold symmetric conformation. *EMBO J* **22:** 4356–4364

Gaczynska M, Osmulski PA, Gao Y, Post MJ, Simons M (2003) Proline- and arginine-rich peptides constitute a novel class of allosteric inhibitors of proteasome activity. *Biochemistry* **42:** 8663–8670

Goldberg AL (2003) Protein degradation and protection against misfolded or damaged proteins. *Nature* **426:** 895–899

Groll M, Bajorek M, Köhler A, Moroder L, Rubin DM, Huber R, Glickman MH, Finley D (2000) A gated channel into the proteasome core particle. *Nat Struct Biol* **7:** 1062–1067

Groll M, Brandstetter H, Bartunik H, Bourenkow G, Huber R (2003) Investigations on the maturation and regulation of archaebacterial proteasomes. *J Mol Biol* **327:** 75–83

Groll M, Ditzel L, Löwe J, Stock D, Bochtler M, Bartunik HD, Huber R (1997) Structure of 20S proteasome from yeast at 2.4 Å resolution. *Nature* **386:** 463–471

Harris CA, Hunte B, Krauss MR, Taylor A, Epstein LB (1992) Induction of leucine aminopeptidase by interferon γ. Identification by protein microsequencing after purification by preparative two-dimensional gel electrophoresis. *J Biol Chem* **267:** 6865–6869

Hoskins JR, Pak M, Maurizi MR, Wickner S (1998) The role of the ClpA chaperone in proteolysis by ClpAP. *Proc Natl Acad Sci USA* **95:** 12135–12140

Hoskins JR, Singh SK, Maurizi MR, Wickner S (2000) Protein binding and unfolding by the chaperone ClpA and degradation by the protease ClpAP. *Proc Natl Acad Sci USA* **97:** 8892–8897

Kisselev AF, Akopian TN, Goldberg AL (1998) Range of sizes of peptide products generated during degradation of different proteins by archaeal proteasomes. *J Biol Chem* **273:** 1982–1989

Knowlton JR, Johnston SC, Whitby FG, Realini C, Zhang ZG, Rechsteiner M, Hill CP (1997) Structure of the proteasome activator REGα (PA28α). *Nature* **390:** 639–643

Köhler A, Cascio P, Leggett DS, Woo KM, Goldberg AL, Finley D (2001) The axial channel of the proteasome core particle is gated by the Rpt2 ATPase and controls both substrate entry and product release. *Mol Cell* **7:** 1143–1152

Lee C, Prakash S, Matouschek A (2002) Concurrent translocation of multiple polypeptide chains through the proteasomal degradation channel. *J Biol Chem* **277:** 34760–34765

Liu CW, Corboy MJ, DeMartino GN, Thomas PJ (2003) Endoproteolytic activity of the proteasome. *Science* **299:** 408–411

Löwe J, Stock D, Jap R, Zwickl P, Baumeister W, Huber R (1995) Crystal-structure of the 20S proteasome from the archaeon *T. acidophilum* at 3.4 Å resolution. *Science* **268:** 533–539

Navon A, Goldberg AL (2001) Proteins are unfolded on the surface of the ATPase ring before transport into the proteasome. *Mol Cell* **8:** 1339–1349

Ortega J, Lee HS, Maurizi MR, Steven AC (2002) Alternating translocation of protein substrates from both ends of ClpXP protease. *EMBO J* **21:** 4938–4949

Osmulski PA, Gaczynska M (2000) Atomic force microscopy reveals two conformations of the 20 S proteasome from fission yeast. *J Biol Chem* **275:** 13171–13174

Osmulski PA, Gaczynska M (2002) Nanoenzymology of the 20S proteasome: proteasomal actions are controlled by the allosteric transition. *Biochemistry* **41:** 7047–7053

Schmitt L, Dietrich C, Tampé R (1994) Synthesis and characterization of chelator lipids for reversible immobilization of engineered proteins at self-assembled lipid interfaces. *J Am Chem Soc* **116:** 8485–8491

Seemüller E, Lupas A, Stock D, Löwe J, Huber R, Baumeister W (1995) Proteasome from *Thermoplasma acidophilum*—a threonine protease. *Science* **268:** 579–582

Singh SK, Grimaud R, Hoskins JR, Wickner S, Maurizi MR (2000) Unfolding and internalization of proteins by the ATP-dependent proteases ClpXP and ClpAP. *Proc Natl Acad Sci USA* **97:** 8898–8903

Stein RL, Melandri F, Dick L (1996) Kinetic characterization of the chymotryptic activity of the 20S proteasome. *Biochemistry* **35:** 3899–3908

Thess A, Hutschenreiter S, Hofmann M, Tampé R, Baumeister W, Guckenberger R (2002) Specific orientation and two-dimensional crystallization of the proteasome at metal-chelating lipid interfaces. *J Biol Chem* **277:** 36321–36328

Uebel S, Tampé R (1999) Specificity of the proteasome and the TAP transporter. *Curr Opin Immunol* **11:** 203–208

Voges D, Zwickl P, Baumeister W (1999) The 26S proteasome: a molecular machine designed for controlled proteolysis. *Annu Rev Biochem* **68:** 1015–1068

Wang J, Hartling JA, Flanagan JM (1997) The structure of ClpP at 2.3 Å resolution suggests a model for ATP-dependent proteolysis. *Cell* **91:** 447–456

Whitby FG, Masters EI, Kramer L, Knowlton JR, Yao Y, Wang CC, Hill CP (2000) Structural basis for the activation of 20S proteasomes by 11S regulators. *Nature* **408:** 115–120

Wickner S, Maurizi MR, Gottesman S (1999) Posttranslational quality control: folding, refolding, and degrading proteins. *Science* **286:** 1888–1893

Zwickl P, Baumeister W (1999) AAA-ATPases at the crossroads of protein life and death. *Nat Cell Biol* **1:** E97–E98

Zwickl P, Grziwa A, Puhler G, Dahlmann B, Lottspeich F, Baumeister W (1992) Primary structure of the *Thermoplasma* proteasome and its implications for the structure, function, and evolution of the multicatalytic proteinase. *Biochemistry* **31:** 964–972

Zwickl P, Lottspeich F, Dahlmann B, Baumeister W (1991) Cloning and sequencing of the gene encoding the large (alpha-) subunit of the proteasome from *Thermoplasma acidophilum*. *FEBS Lett* **278:** 217–221